Organic Electronics 58 (2018) 207–215

Contents lists available at ScienceDirect

Organic Electronics

journal homepage: www.elsevier.com/locate/orgel

A building-block approach to the development of an equivalent circuit model for organic photovoltaic cells

Elisa Sesa[a,b], Ben Vaughan[a], Krishna Feron[a], Chhinder Bilen[a], Xiaojing Zhou[a], Warwick Belcher[a], Paul Dastoor[a,*]

[a] Centre for Organic Electronics, University of Newcastle, Newcastle, NSW, 2308, Australia
[b] Center of Organic Electronics, Universitas Tadulako, Palu, 94118, Indonesia

ARTICLE INFO

Keywords:
Organic photovoltaic cells (OPV)
Equivalent circuit model
And degradation

ABSTRACT

A novel approach to equivalent circuit modelling of organic photovoltaic (OPV) cells capable of simulating both optimal and degraded devices has been developed. Freshly made OPVs (composed of an active layer with a blended poly (3-hexylthiophene) (P3HT) and indene-C60 bisadduct (ICBA) film), that exhibit a characteristic 'J' shaped current-voltage (I-V) curve both in the dark and under illumination, are typically fitted to a one-diode equivalent circuit model. However, as device performance deteriorates, the I-V curve undergoes a series of changes resulting in the evolution of an 'S' shaped I-V curve, for which there is no widely accepted equivalent circuit model. Here we present a building-block approach to develop a simple equivalent circuit model which provides an excellent fit to experimental I-V data spanning the continuum from the ideal 'J' to degraded 'S' shaped curves. Applying this new model to P3HT:ICBA devices provides insights into the physical processes that occur during degradation.

1. Introduction

Organic photovoltaic (OPV) cells are an established solar energy conversion technology that are light-weight, flexible and can be easily fabricated at low cost [1–6]. Understanding the underlying physics of the OPV power conversion process is essential to determine the limiting factors that hinder their efficiency. One approach is to understand the electrical behaviour of OPVs when modelled with an equivalent electrical circuit. The most common equivalent electrical circuit used to model OPVs is the one diode model (ODM) [7–10]. This model has been adapted from inorganic photovoltaic cells (IPVCs), where it is derived by considering their electrical behaviour as a p-n junction [11]. The application of the ODM to OPVs seems reasonable given that bulk heterojunction OPVs consist of a p-type organic material (acting as an electron donor) blended with an n-type organic material (acting as an electron acceptor) to form an intermixed array of p-n junctions [12,13].

Although the ODM has been widely applied to OPVs, it is unable to account for all of the features of the OPV current-voltage (I-V) characteristics. In particular, a common feature of these I-V characteristics is the presence of a kink, which produces an 'S' shaped I-V curve. In these circumstances, the ODM is simply incapable of fitting the I-V characteristic. The kink reduces the fill factor (FF) which in turn lowers the power conversion efficiency (PCE) of the OPVs [14]. The cause of this behaviour has been variously attributed to cathode evaporation resulting in a low quality interface [15], cathode oxidation [16], oxygen diffusion into the device through an aluminium cathode [16], charge accumulation [17], imbalance in mobility of the charge carriers [18], restricted charge transport at interfaces [19,20], photodesorption and oxygen redistribution [21], and hole-transport limitations in the donor (hole transport) layer [22]. Other reports have suggested the S-shaped curve is caused by interfacial dipoles, defects, and traps [23]. Dynamic Monte Carlo modelling further shows that efficient organic photovoltaic systems are more susceptible to exhibiting 'S' shaped I-V curves due to interface effects [24].

Over the past decade or so, several authors have proposed modifications to the ODM to better describe the S-shaped electrical behaviour of OPVs, with an excellent review reported recently [25]. In 2006, Mazhari proposed a 3-diode model to describe a voltage-dependent photocurrent in OPV devices [26]. The first attempt to model 'S'-shaped I-V curves in OPVs directly was described in 2008 using a 2-diode model by de Castro et al. [27]. In 2010, del Pozo et al. [28] used de Castro's model to extract the electrical parameters of 'S' shaped I-V curves in polymer/fullerene OPVs. But none of these models are capable of fitting the full voltage range of the OPV's I-V curve, especially the quadrant beyond V_{oc}, which is related to the series resistance of the cells. In 2013, García-Sánchez et al. proposed a solution to fitting the I-

* Corresponding author.
E-mail address: Paul.Dastoor@newcastle.edu.au (P. Dastoor).

https://doi.org/10.1016/j.orgel.2018.04.019
Received 5 January 2018; Received in revised form 9 April 2018; Accepted 10 April 2018
Available online 11 April 2018

V curve far beyond V_{oc} through the addition of a third diode [29]. In 2016, a further modification of this 3-diode model was proposed by de Castro et al. who included an additional shunt resistance and removed the associated series resistance [30].

Previous work in this laboratory has focussed on developing a new building block approach to modelling OPV devices [31]. This model has already been implemented by others, for example, Furchi et al. have used it to explain the behaviour of MoS_2: WSe_2 cells and other cells where the photocurrent generation relies on high exciton binding energies [32]. In addition, Pozza et al. have used this model to characterise the response of R2R printed P3HT:PCBM devices tested under ISOS conditions [33]. However, a complete description of the model, including the origin of the building block approach, has yet to be reported.

In light of the interest in this new model, in this paper we detail fully our building-block approach to the development of an equivalent circuit model for OPV devices. In particular, we show how we start by identifying the key features of the I-V curve and then discuss how discrete circuit elements can be used to fit these features. Using this approach, we demonstrate that it is now possible to fit the full OPV I-V curve using the minimum number of circuit elements. Finally, we apply the new model to the degradation of OPV devices and show that the model provides physical insights into the degradation process.

2. Experimental details

2.1. Device fabrication

Patterned indium tin oxide (ITO) substrates were cleaned in an ultrasonic bath using detergent, acetone and iso-propanol. After drying the slides, a 75 µl filtered poly (3,4-ethylenedioxythiophene)/(poly (styrenesulfonate) (PEDOT:PSS, Baytron P) solution was spin-coated onto each ITO slide at 4000 rpm for 90 s. The slides were then dried in an oven at 140 °C for 30 min. The active layer solution for the BHJ devices was prepared by blending the poly (3-hexylthiophene) (P3HT) with a novel indene-C60 bisadduct (ICBA, Lumtec Corp.) in a 1:0.8 ratio. The blend was dissolved in a chloroform solution at a concentration of 18 mg/ml and sonicated for 60 min. The P3HT: ICBA BHJ blend was spin coated onto the ITO/PEDOT: PSS substrates, which were then dried on a hot plate at 50 °C for 4 min in a nitrogen glove box. These active layers were then transferred into a vacuum chamber for electrode evaporation. A calcium/aluminium cathode (Ca = 20 nm, Al = 90 nm) was then evaporated on top of the active layer. Eight individually addressable devices were fabricated on each substrate, with the active area of each device (determined by the overlap between the ITO and the metal) being approximately 14 mm^2.

2.2. Device characterization

The devices were firstly annealed on a hot plate at 140 °C for 4 min. Then four devices (Fig. 1, devices 3, 4, 5 and 6) were encapsulated using PVC tape as a protection layer from humidity and oxygen ingress, and the remaining four devices (Fig. 1, devices 1, 2, 7 and 8) left unencapsulated. Continuous photocurrent-voltage (I-V) measurements were conducted every hour under ambient conditions using a 12 V halogen lamp to illuminate all eight devices. The light intensity was measured to be 100 mW/cm^2 by a silicon reference solar cell (FHG-ISE). The I-V data of each device were automatically recorded for several days.

3. Development of the equivalent circuit model

The ideal (or 'J'-shaped) photovoltaic I-V curve has been described traditionally using the ODM (Fig. 2).

Using this equivalent circuit model, the total current is given by:

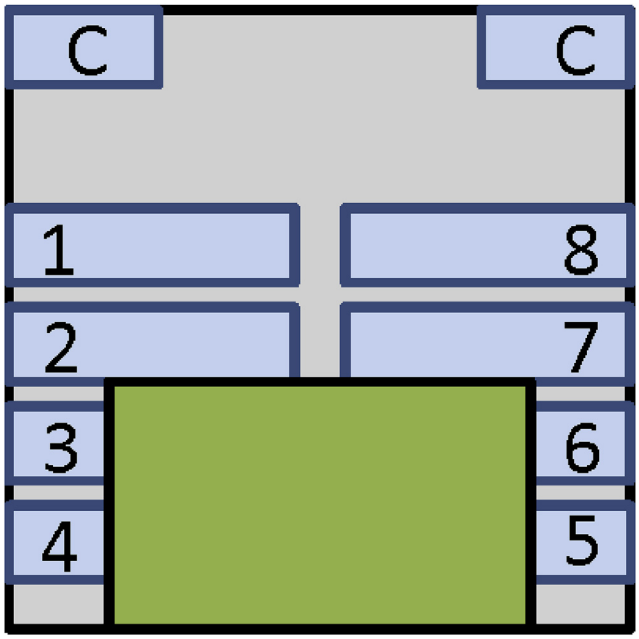

Fig. 1. Schematic drawing of the OPV device geometry and degradation study. Each substrate has 8 individual devices (electrodes 1–8) and a common contact (electrode C). Devices 3, 4, 5 and 6 were encapsulated as shown by the green area and devices 1, 2, 7 and 8 were left unencapsulated. (For interpretation of the references to colour in this figure legend, the reader is referred to the Web version of this article.)

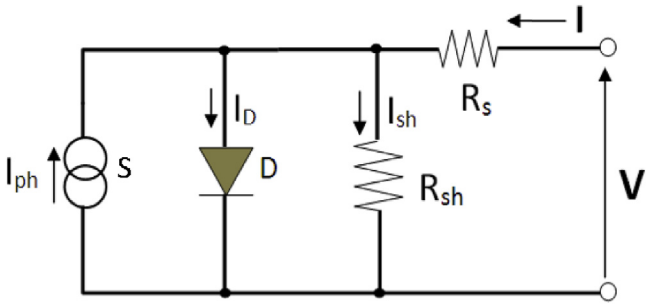

Fig. 2. The ODM equivalent circuit, incorporating a current source, S, diode, D, shunt resistance, R_{sh} and series resistance, R_s.

$$I = -I_{ph} + I_D + I_{sh} \tag{1}$$

where I_{ph}, I_D, and I_{sh} are the photocurrent, diode current and shunt current respectively. Thus, by substituting expressions for the diode equation and the shunt current this expression can be expanded to give the well-known ODM:

$$I = -I_{ph} + I_0\left[\exp\left(\frac{q(V - IR_s)}{nkT}\right)\right] + \frac{V - IR_s}{R_{sh}} \tag{2}$$

where k, T, q are the Boltzmann constant, temperature, and the elementary charge, respectively. The main parameters I_o, I_{ph}, n, R_s, and R_{sh} are the saturation current of the diode D, the photocurrent, the ideality factor of the diode, the series resistance, and the shunt resistance, respectively. For optimised OPV devices, Equation (2) provides a good fit to the ideal 'J'-shaped diode characteristics.

However, the need for a new approach to the development of an equivalent circuit model for OPVs is perhaps best illustrated in Fig. 3, which shows the I-V characteristic for an as-fabricated OPV device (Fig. 3 (a)) and an OPV device fabricated under the same conditions following exposure to ambient air (Fig. 3 (b)). These two plots highlight the fact that the OPV I-V characteristic transitions from the ideal 'J'-

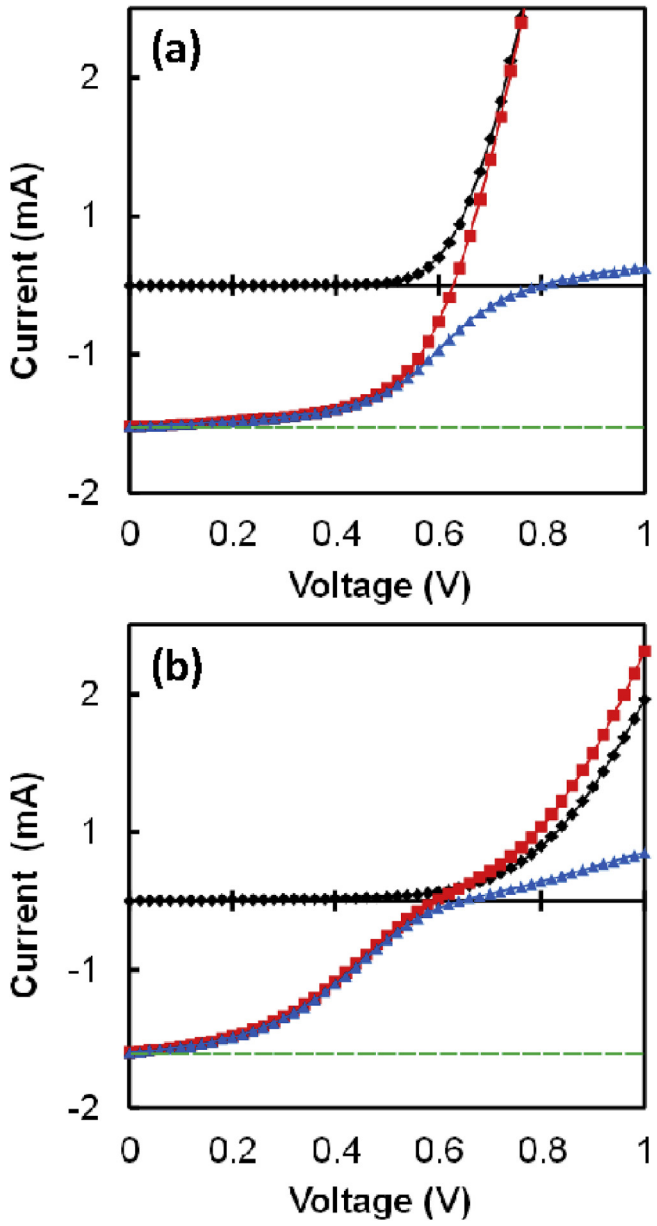

Fig. 3. Current-voltage (I–V) characteristics of: (a) an optimised 'J' shaped OPV device and (b) a degraded 'S' shaped device. Both plots show the variation of the dark current, I_{dark} (black diamonds), the light current, I (red squares), the difference between the light and dark currents, $I - I_D$ (blue triangles) and the ideal photocurrent, I_{ph} (green dashes) respectively. (For interpretation of the references to colour in this figure legend, the reader is referred to the Web version of this article.)

shape to a 'S'-shape associated with degraded devices [15,21,23].

Equation (2) indicates that the difference between the dark current ($I_{dark} = I_D + I_{sh}$) and the current under illumination (light current, I) is given by I_{ph}, which is independent of voltage and thus should follow the ideal relationship shown by the green dashed line in Fig. 3 (a). However, the difference between light and dark currents (as shown by the blue triangles in Fig. 3 (a)) clearly demonstrates that I_{ph} actually exhibits a voltage dependent behaviour, which was first discussed by Mazhari [26]. Thus, whilst the ODM can be made to approximate the illuminated I-V characteristic, it is clear that even in the case of an apparently ideal OPV device, the ODM is not an accurate physical model of OPV behaviour and the parameters obtained will not necessarily reflect the actual device characteristics accurately. Moreover, the deviation from the ODM increases with voltage and becomes most significant in the region around V_{oc} and beyond. Furthermore, the discrepancy between the ideal and actual $I - I_{dark}$ values becomes more pronounced as the I-V characteristic tends towards 'S'-shaped until the ODM is simply unable to fit the I-V curve at all.

Fig. 3 implies that all OPV I-V curves exist on a continuum between the 'J'-shaped and 'S'-shaped characteristics. In other words, all OPV I-V characteristics contain some 'S'-shaped character and as such accurately modelling the 'S' shaped curve is essential to ensure that the physical parameters that are obtained from the fit are meaningful.

In its most general sense, the 'S'-shaped I-V characteristic consists of a sigmoidal function where the inflection point is arbitrarily offset from the current and voltage axes. Consequently, the circuit elements required to model this function must be capable of generating a sigmoidal function with the required current and voltage offset. Previous work by White et al. has shown that two 'back-to-back' diodes are the simplest circuit element required to model a sigmoidal function [34]. This configuration was used to model the nonlinear effect of metal-semiconductor junctions formed between fused-silica insulators and the platinum of the standard platinum resistance thermometers (SPRT) sensing element and lead wires [35].

Fig. 4 shows a circuit element based on two ideal 'back-to-back' diodes (D_1 and D_2) and a shunt resistor R_{sh} as well as a typical output characteristic for this circuit. The functional form for the current flowing in this equivalent circuit is given by:

$$I = \frac{I_{01}I_{02}[\exp(qV/kT) - 1]}{I_{01}\exp(qV/kT) + I_{02}} + \frac{V}{R_{sh}} \tag{3}$$

where I_{01} and I_{02} are the saturation currents for D_1 and D_2, respectively.

As expected, the I-V characteristic exhibits the required sigmoidal shape but the inflection point necessarily passes through the origin.

In order to provide the current offset, a constant current source is added to the equivalent circuit, as shown in Fig. 5. The associated I-V characteristic shows that the constant current source provides the required displacement of the inflection point from the current axis.

The functional form for the current flowing in the modified equivalent circuit is then given by:

$$I = -I_{ph} + \frac{I_{01}I_{02}[\exp(qV/kT) - 1]}{I_{01}\exp(qV/kT) + I_{02}} + \frac{V}{R_{sh}} \tag{4}$$

In order to provide the required voltage offset, a constant voltage source is added to the equivalent circuit, as shown in Fig. 6. The associated I-V characteristic shows that the constant voltage source provides the required displacement of the inflection point from the voltage axis.

The addition of this constant voltage source results in a functional form for the current flowing in the modified equivalent circuit as follows:

$$I = -I_{ph} + \frac{I_{01}I_{02}[\exp(q\,(V - V_{offset})/kT) - 1]}{I_{01}\exp(q\,(V - V_{offset})/kT) + I_{02}} + \frac{V - Voffset}{R_{sh}} \tag{5}$$

Fig. 6 shows that we have now successfully developed the circuit elements required to produce a sigmoidal I-V characteristic where the inflection point is arbitrarily offset from the current and voltage axes in the fourth quadrant. However, in order to reproduce the full I-V characteristic of an actual OPV device, the circuit elements in Fig. 6 need to be combined with the diode and shunt and series resistors of the ODM. As such, the circuit elements in Fig. 6 effectively become a modified version of the constant current source in the original ODM. Furthermore, the resistor, R, can be eliminated without loss of generality resulting in the complete circuit structure and the corresponding typical I-V output characteristic illustrated in Fig. 7.

The current-voltage characteristic of the complete equivalent circuit under illumination is given by the following equation:

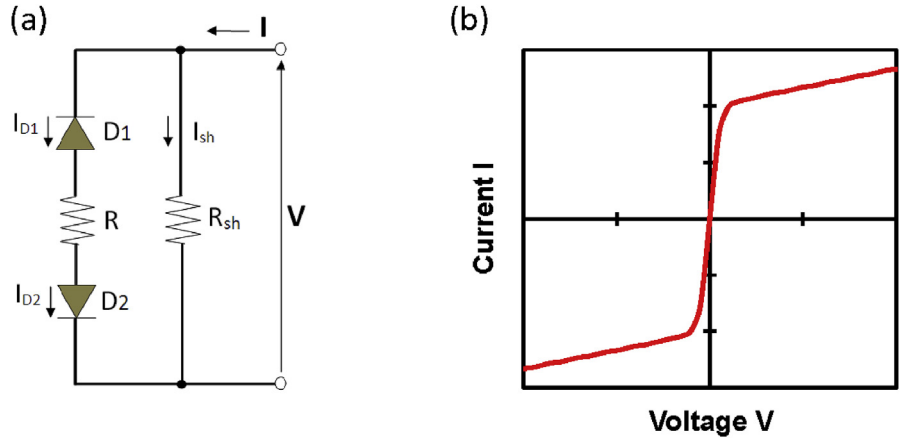

Fig. 4. (a) The back-to-back diode circuit element, and (b) the corresponding typical sigmoidal I-V output characteristic.

$$I = -I_{ph} + \frac{V - IR_s - V_{offset}}{R_{sh1}} + \frac{I_{01}I_{02}\left[\exp\left(\frac{q(V-IR_s-V_{offset})}{kT}\right) - 1\right]}{I_{01}\exp\left(\frac{q(V-IR_s-V_{offset})}{kT}\right) + I_{02}} + I_{03}\left[\exp\left(\frac{q(V-IR_s)}{nkT}\right) - 1\right] + \frac{V - IR_s}{R_{sh2}} \quad (6)$$

The modified current source now more accurately represents the corrected photocurrent I_{ph^*} of non-ideal OPVs and exhibits the observed 'S' shaped I-V characteristic when the OPV is operated under certain illumination conditions. From Equation (6) the corrected photocurrent I_{ph^*} is given by:

$$I_{ph*} = -I_{ph} + \frac{V - IR_s - V_{offset}}{R_{sh1}} + \frac{I_{01}I_{02}\left[\exp\left(\frac{q(V-IR_s-V_{offset})}{kT}\right) - 1\right]}{I_{01}\exp\left(\frac{q(V-IR_s-V_{offset})}{kT}\right) + I_{02}} \quad (7)$$

4. Results and discussion

In order to assess the ability of the new equivalent circuit to model the I-V performance of both 'J' and 'S' shaped devices, a series of encapsulated and unencapsulated devices were fabricated and characterised. Fig. 8 shows the I-V characteristics of encapsulated and unencapsulated devices as a function of exposure time to ambient conditions, with the device parameters summarized in Table 1. While both encapsulated and unencapsulated devices exhibit a similar initial device performance with respect to open circuit voltage (V_{oc}), short circuit current (I_{sc}), fill factor (FF), and efficiency (PCE) as shown in Table 1, all of them degrade over time. As expected, the degradation process of the unencapsulated cells exhibits a systematically faster reduction of J_{sc}, FF, and PCE. After 156 h of continuing measurement, the I_{sc}, FF, and PCE have dropped to 14%, 76% and 11% of their original values and a pronounced 'S'-shaped I-V curve is observed. The similar reduction rates of I_{sc} and PCE indicate that the loss of photocurrent is the major factor decreasing the device performance. A 25% reduction in the FF after 156 h can be attributed to a reduction in shunt resistance and an increase in series resistance [36]. In contrast, although the encapsulated device also degraded, it didn't develop an 'S' shaped I-V characteristic as quickly as its unencapsulated counterpart. As such, the evolution of the 'S' shaped I-V characteristic is not due to light exposure only but rather must be attributed to an oxidation process.

The transition from the 'J' to the 'S' shaped I-V characteristic with exposure time is illustrated in Fig. 9. The as-fabricated unencapsulated device starts with an ideal 'J' shaped curve (Fig. 9 (a)) and only starts to show a 'S'-shaped I-V characteristic after 48 h of exposure (Fig. 9 (b)), which becomes most pronounced after 72 h (Fig. 9 (c)). By comparison, for the encapsulated device (not shown), a 'S'-shape I-V curve is not observed until 156 h of continuous illumination.

In order to demonstrate the quality of the new model fits to the degraded 'S' shaped curves we need to compare them to the quality of fit of the ODM. In particular, it is necessary to determine whether the new model is over parameterized with respect to the ODM, that is, if the quality of the fits are equally correct using fewer parameters. In the case of fitting problems where one model's parameters are nested within the other, this assessment can be achieved by means of a statistical F-test based on the residual sum of squares of the two models and their degrees of freedom [37,38]. The new model fit was applied to the J-V data that exhibited a perceptible 'S'-shaped nature and F-test values were calculated in these cases (see Supplementary Material). For the

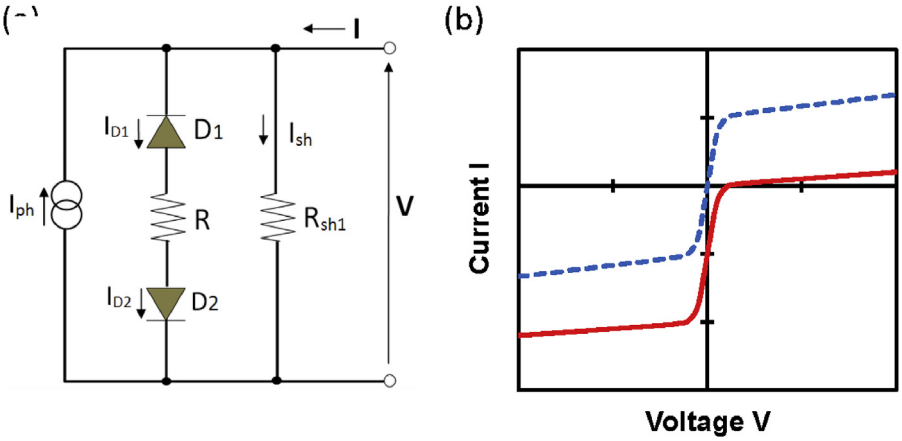

Fig. 5. (a) The electrical circuit containing the back-to-back diode circuit element and constant current source, I_{ph}. (b) The corresponding typical I-V output characteristics before (blue dashed line) and after (red solid line) adding the constant current source, I_{ph}. (For interpretation of the references to colour in this figure legend, the reader is referred to the Web version of this article.)

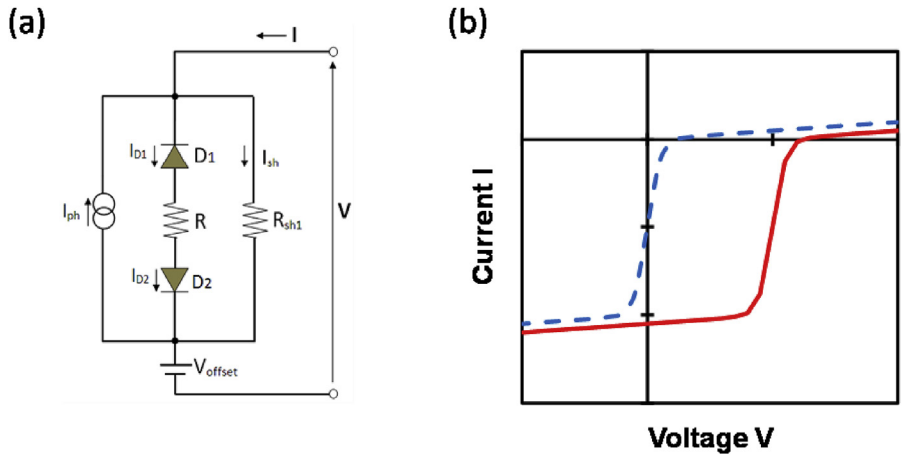

Fig. 6. (a) The electrical circuit containing the back-to-back diode circuit element, constant current source, I_{ph} and offset voltage *Voffset* (b) The corresponding typical I-V output characteristics before (blue dashed line) and after (red solid line) adding the offset voltage *Voffset*. (For interpretation of the references to colour in this figure legend, the reader is referred to the Web version of this article.)

remaining data only the ODM was applied. The fitted parameters have been extracted and summarized in Table 2 and the fitting results are shown in Fig. 10 (a) and 10 (b). The percentage error between the experimental current, I_{exp} and the model-fit current, I_{model} were calculated using the following equation:

$$\%\ Error = 100 \times \frac{|I_{\exp} - I_{\mathrm{mod}\,el}|}{I_{\mathrm{mod}\,el}} \tag{8}$$

and are shown as a function of applied voltage in Fig. 10 (c) and 10 (d).

In Table 2 the grey shaded rows denote data fitted by the ODM using equation (2) whereas all remaining rows are fitted by the new model using equation (7). In all cases, the F value indicates that the new model fit is statistically superior to that of the ODM. Both models provide sensible values for the fitted parameters, with for example R_s and R_{sh} values of 51–86 Ω and 47–200 kΩ respectively. The fitted values for the ideality factor range between 5 and 11; consistent with many preceding studies using equivalent circuit modelling of organic photovoltaic cells with values ranging from 0.6 to 20 reported [39–42]. Recent work by Tvingstedt and Deibel has identified that the ideality factor in OPV is difficult to correctly determine due to the influence of resistive losses in the device; resulting in fitted ideality factors greater than unity [41]. Consequently, ideality factors that deviate from unity are not an indication of a poor model fit but rather that the ideality factor acts a proxy term for the complex loss processes that occur in these devices [42]. Interestingly, the difference between the offset voltage, V_{offset}, and the open circuit voltage, V_{oc}, increases systematically with device degradation time; consistent with the development of an intrinsic dipole within the device associated with space-charge limited transport [23].

Fig. 10 (c) and 10 (d) show the percentage error resulting from the deviation of both models from the experimental data as a function of device voltage. Both models fit the experimental data very well, with a maximum percentage error of < 10% in all cases, demonstrating that the new model fits 'S' shaped data as well as, or better than, the conventional ODM fits ideal 'J' shaped data and giving validation to the new model. Interestingly, in all cases the maximum deviation of the models from the experimental data occurs in the same two regions which straddle the knee in the 'J' shaped data; at ~600 mV and just above V_{oc} at ~850 mV. Both the ODM and the new model contain a common diode element (D in Fig. 2 and D3 in Fig. 7 respectively) responsible for fitting the 'J' shaped character present in both pristine and degraded devices. As such, the observation that the absolute error in these regions is the same for both the ODM and the new model suggests that this discrepancy is a result of the common diode component being unable to adequately fit the 'J' shaped component of the experimental data [43], rather than an error associated with new model's fitting of the 'S' shaped kink in in the degraded data sets.

It is well-established that the physics of device degradation leading to S-shaped curves is a consequence of charge accumulation and dipole formation at one or other electrode [44–49]. Indeed, this behaviour is typically contained within drift diffusion modelling of OPV devices through the inclusion of an electrical field term arising from the accumulated charge [23]. This dipole electric field effectively reduces the in-built electric field (originating from the work function difference between the two electrodes) and hence reduces the photocurrent through an increase in charge recombination [50]. Thus, in order for any equivalent electrical circuit to successfully model this current-voltage behaviour it must take into account this dipole formation and the corresponding electric field change that occurs at the electrodes.

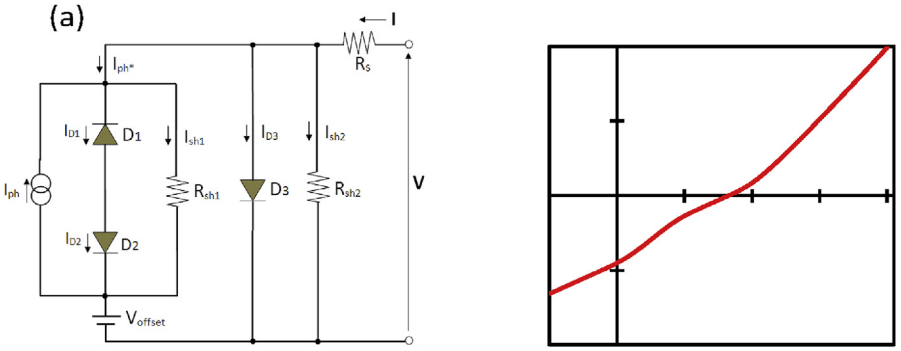

Fig. 7. (a) The electrical circuit containing the modified current source together with the diode, D_3, and series and shunt resistances, R_s, and R_{sh2}. (b) The corresponding typical I-V output characteristics of the complete new OPV equivalent circuit.

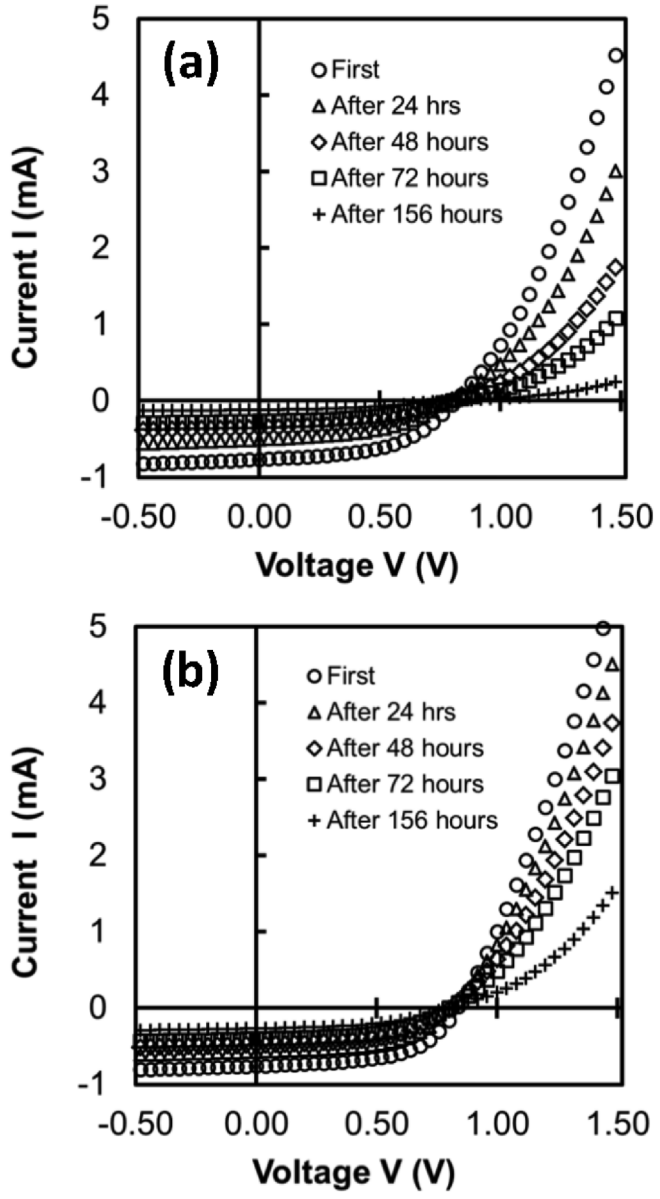

Fig. 8. Variation of I-V characteristic as a function of exposure time to ambient conditions for: (a) unencapsulated, and (b) encapsulated devices.

Table 1
A summary of measured OPV device performance.

Sample	Degradation time (hours)	Device parameters			
		V_{oc} (V)	I_{sc} (mA)	FF	η (%)
Unencapsulated	0	0.833	0.86	0.525	2.7
	24	0.794	0.51	0.472	1.4
	48	0.802	0.36	0.468	1.0
	72	0.823	0.27	0.443	0.7
	156	0.804	0.12	0.401	0.3
Encapsulated	0	0.838	0.76	0.561	2.6
	24	0.812	0.58	0.535	1.8
	48	0.807	0.48	0.523	1.5
	72	0.807	0.40	0.512	1.2
	156	0.825	0.27	0.464	0.7

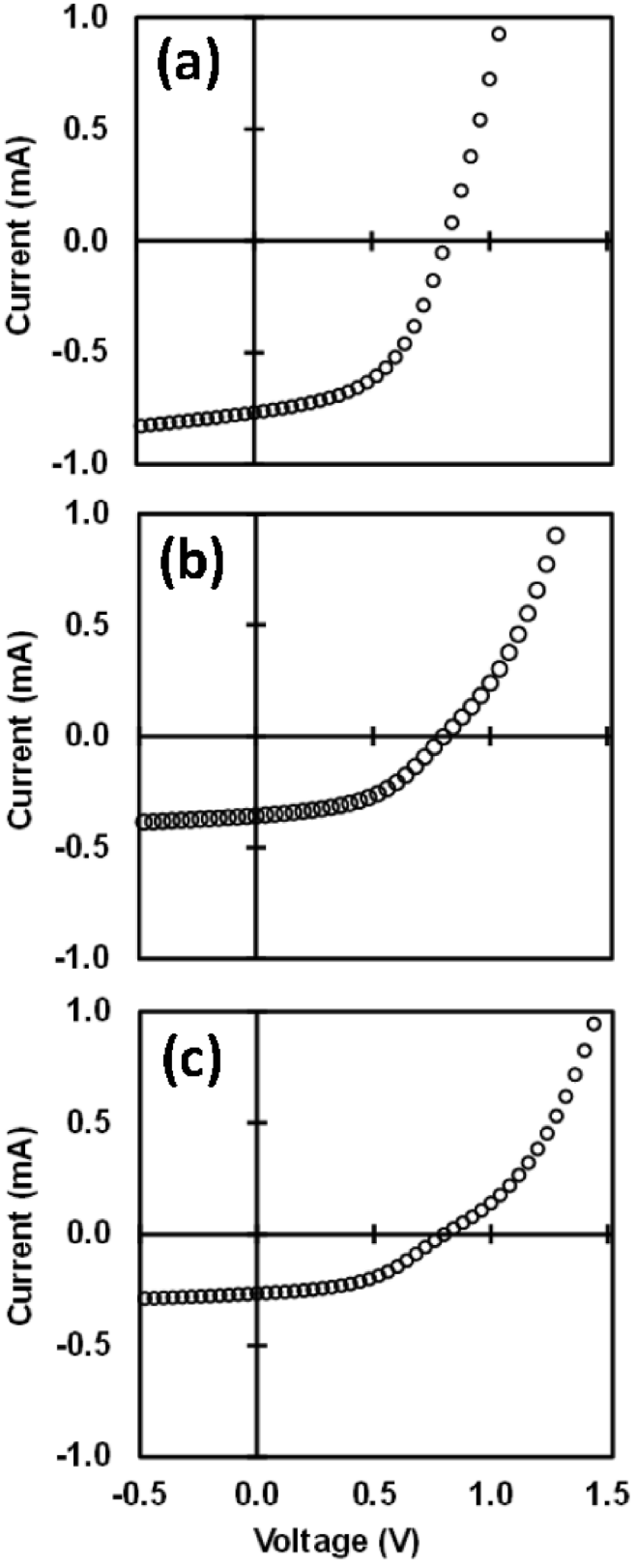

Fig. 9. Separated I–V curves of the unencapsulated cell shows the cell pronounced S-shaped curve in the degradation process. a) initial measurement, b) after 48 h, and c) after 72 h.

Table 2
The parameters extracted from the best fit-to-data for unencapsulated devices.

Device type	Degradation time (hours)	Model-fitted parameters									
		I_{o1} (mA)	I_{o2} (mA)	I_{o3} (mA)	I_{ph} (mA)	n_3	R_s (Ω)	R_{sh1} (Ω)	R_{sh2} (Ω)	V_{offset} (V)	F-value
Unencapsulated	0	–	–	0.018	0.790	8	54	–	59903	–	–
	24	–	–	0.029	0.524	11	51	–	57705	–	–
	48	0.048	0.057	0.011	0.287	10	61	30000	60000	0.68	415
	72	0.027	0.077	0.006	0.217	10	76	30000	60000	0.62	550
	156	0.032	0.028	0.002	0.068	10	81	30000	200000	0.58	1038
Encapsulated	0	–	–	0.001	0.777	5	74	–	59932	–	
	24	–	–	0.002	0.585	6	79	–	47459	–	
	48	–	–	0.004	0.492	7	81	–	59606	–	
	72	0.048	0.040	0.003	0.335	7	86	30000	60000	0.79	15
	156	0.048	0.038	0.005	0.203	9	85	30000	60000	0.70	44

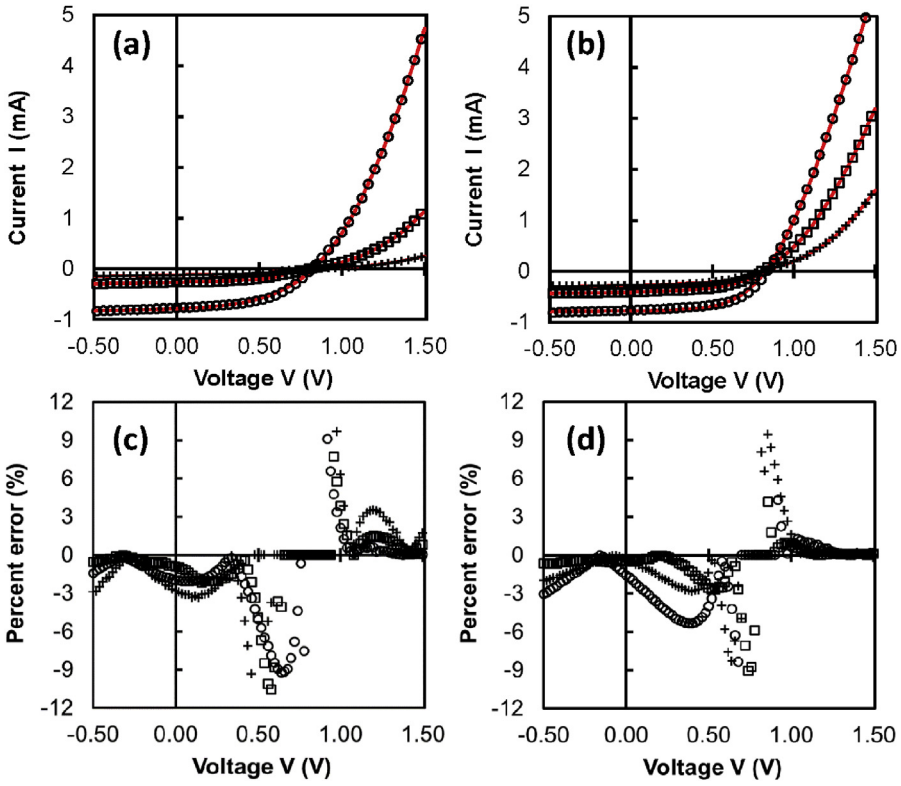

Fig. 10. The experimental (symbols) and model-fitted *I–V* curves (red solid lines) using the one diode model and the modified equivalent circuit model for: (a) unencapsulated and (b) encapsulated cells. Degradation times of 0 h (open circles), 72 h (open squares) and 156 h (crosses) are shown. Panels (c) and (d) show the percentage error between the experimental current and model-fit current for the three degradation times for the unencapsulated and encapsulated cells, respectively. (For interpretation of the references to colour in this figure legend, the reader is referred to the Web version of this article.)

However, to date, none of the current equivalent circuit models directly account for this phenomenon. In the new model presented in this paper, the presence of the interfacial charge accumulation that drives S-shape formation is directly accounted for by the addition of the interface voltage source, V_{offset} and two semiconducting junctions, D_1 and D_2. In other words, the key insight delivered by the new equivalent circuit model is that the physical origins of the degraded I-V curve lie in the generation of a new internal field, arising from the voltage source V_{offset}, as well as the creation of two new semiconducting junctions, D_1 and D_2, which are distinct from the diode behaviour that arises from the donor-acceptor junctions established in the active layer of the device. These new equivalent circuit components act to reduce the photocurrent generated by the solar cell with increasing applied voltage; consistent with the conventional description of a space-charge limited current in degraded devices [36].

Another way of visualising this effect is shown in Fig. 11 (a) and (b), which plot the differential resistance in the device as a function of applied voltage. A clear peak is observed in the differential resistance located at an applied voltage of ~0.88 V that grows systematically with increasing degradation time; reflecting the inflection point position (kink) of the S-shaped I-V curve. As such, this peak is consistent with the presence of residual charge located at one of the electrode interfaces modelled by D_1 or D_2.

Previous work by Feron et al. [51] has shown that aluminium oxidation at the Al/active layer interface dominates during degradation and effectively reduces the photocurrent. Furthermore, De Castro et al. showed that the kink is related to defect states at the cathode-organic layer interface [24,27], while Kumar argued the S-shaped kink can be attributed to the presence of a strong interface dipole [23]. Consequently, the main degradation process reflected by the new model corresponds to oxidation of the cathode. This conclusion is consistent with circuit elements D_1 and D_2 being associated with the electrode/semiconductor interfaces at the anode and cathode, while V_{offset} results from the dipole that is established at the cathode/active layer interface due to the intrinsic space charge that occurs in a degraded device at low internal applied fields close to V_{oc}.

5. Conclusions

A new equivalent circuit model for organic photovoltaic devices has

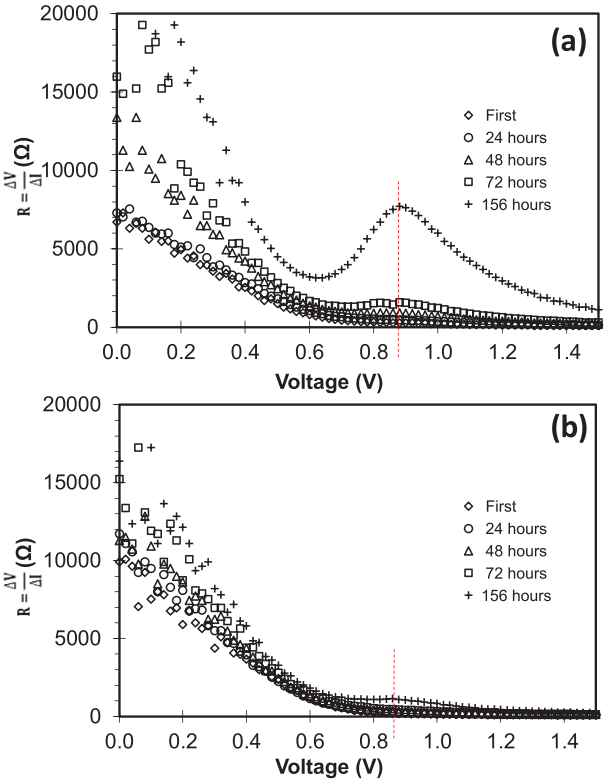

Fig. 11. Plot of differential resistance as a function of applied voltage for: (a) unencapsulated and (b) encapsulated devices. The dashed red line indicates the position of the peak in the differential resistance. (For interpretation of the references to colour in this figure legend, the reader is referred to the Web version of this article.)

been developed. The new model utilises three diodes and an in-built voltage offset term to allow degraded devices to be accurately simulated, whilst reducing to the conventional one-diode model when applied to non-degraded pristine devices. Adopting a building-block approach to fitting the shape of the degraded I-V curve intrinsically minimises the number of active circuit elements in the model. Here we apply the model to the well-established degradation of ITO/PEDOT:PSS/P3HT:ICBA/Al devices and show that the model provides new physical insights into the nature of the degradation processes. In particular, we show that the circuit elements can be associated with physical process that occur at the electrode interfaces and within the bulk-heterojunction.

Appendix A. Supplementary data

Supplementary data related to this article can be found at http://dx.doi.org/10.1016/j.orgel.2018.04.019.

References

[1] C.J. Brabec, N.S. Sariciftci, J.C. Hummelen, Plastic solar cells, Adv. Funct. Mater. 11 (2001) 15–26.
[2] C.J. Brabec, Organic photovoltaics: technology and market, Sol. Energy Mater. Sol. Cells 83 (2004) 273–292.
[3] K.M. Coakley, M.D. McGehee, Conjugated polymer photovoltaic cells, Chem. Mater. 16 (2004) 4533–4542.
[4] E. Bundgaard, F.C. Krebs, Low band gap polymers for organic photovoltaics, Sol. Energy Mater. Sol. Cells 91 (2007) 954–985.
[5] G.J. Hedley, A. Ruseckas, I.D.W. Samuel, Light harvesting for organic photovoltaics, Chem. Rev. 117 (2017) 796–837.
[6] P. Mao, Y. Wei, H. Li, J. Wang, Junction diodes in organic solar cells, Nanomater. Energy 41 (2017) 717–730.
[7] S. Yoo, B. Domercq, B. Kippelen, Intensity-dependent equivalent circuit parameters of organic solar cells based on pentacene and C_{60}, J. Appl. Phys. 97 (2005) 103706.
[8] A. Moliton, J.-M. Nunzi, How to model the behaviour of organic photovoltaic cells, Polym. Int. 55 (2006) 583–600.
[9] A. Cheknane, H.S. Hilal, F. al Djeffal, B. Benyoucef, J.-P. Charles, An equivalent circuit approach to organic solar cell modelling, Microelectron. J. 39 (2008) 1173–1180.
[10] W.J. Potscavage, A. Sharma, B. Kippelen, Critical interfaces in organic solar cells and their influence on the open-circuit voltage, Acc. Chem. Res. 42 (2009) 1758–1767.
[11] W. Shockley, Bell System Technical Journal 28 (1949) 435–489.
[12] P.W.M. Blom, V.D. Mihailetchi, L.J.A. Koster, D.E. Markov, Device physics of polymer:fullerene bulk heterojunction solar cells, Adv. Mater. 19 (2007) 1551–1566.
[13] B. Kippelen, J.-L. Bredas, Organic photovoltaics, Energy Environ. Sci. 2 (2009) 251–261.
[14] M. Glatthaar, M. Riede, N. Keegan, K. Sylvester-Hvid, B. Zimmermann, M. Niggemann, A. Hinsch, A. Gombert, Efficiency limiting factors of organic bulk heterojunction solar cells identified by electrical impedance spectroscopy, Sol. Energy Mater. Sol. Cells 91 (2007) 390–393.
[15] D. Gupta, M. Bag, K.S. Narayan, Correlating reduced fill factor in polymer solar cells to contact effects, Appl. Phys. Lett. 92 (2008) 093301.
[16] D. Cheyns, H. Gommans, M. Odijk, J. Poortmans, P. Heremans, Stacked organic solar cells based on pentacene and C_{60}, Sol. Energy Mater. Sol. Cells 91 (2007) 399–404;
a F.C. Krebs, K. Norrman, Analysis of the failure mechanism for a stable organic photovoltaic during 10 000 h of testing, Prog. Photovoltaics Res. Appl. 15 (2007) 697–712.
[17] J.C. Wang, X.C. Ren, S.Q. Shi, C.W. Leung, P.K.L. Chan, Charge accumulation induced S-shape J–V curves in bilayer heterojunction organic solar cells, Org. Electron. 12 (2011) 880–885.
[18] W. Tress, A. Petrich, M. Hummert, M. Hein, K. Leo, M. Riede, Imbalanced mobilities causing S-shaped IV curves in planar heterojunction organic solar cells, Appl. Phys. Lett. 98 (2011) 063301.
[19] W. Tress, O. Inganäs, Simple experimental test to distinguish extraction and injection barriers at the electrodes of (organic) solar cells with S-shaped current–voltage characteristics, Sol. Energy Mater. Sol. Cells 117 (2013) 599–603.
[20] A. Wagenpfahl, D. Rauh, M. Binder, C. Deibel, V. Dyakonov, S-shaped current-voltage characteristics of organic solar devices, Phys. Rev. B 82 (2010) 115306.
[21] M.R. Lilliedal, A.J. Medford, M.V. Madsen, K. Norrman, F.C. Krebs, The effect of post-processing treatments on inflection points in current–voltage curves of roll-to-roll processed polymer photovoltaics, Sol. Energy Mater. Sol. Cells 94 (2010) 2018–2031.
[22] M. Zhang, H. Wang, C.W. Tang, Hole-transport limited S-shaped I-V curves in planar heterojunction organic photovoltaic cells, Appl. Phys. Lett. 99 (2011) 213506.
[23] A. Kumar, S. Sista, Y. Yang, Dipole induced anomalous S-shape I-V curves in polymer solar cells, J. Appl. Phys. 105 (2009) 094512.
[24] K. Feron, X. Zhou, W.J. Belcher, C.J. Fell, P.C. Dastoor, A dynamic Monte Carlo study of anomalous current voltage behaviour in organic solar cells, J. Appl. Phys. 116 (2014) 214509.
[25] F.J. García-Sánchez, B. Romero, D.C. Lugo-Muñoz, G. Del Pozo, B. Arredondo, J.J. Liou, A. Ortiz-Conde, Modelling solar cell S-shaped I-V characteristics with DC lumped-parameter equivalent circuits – a review, FU Elect. Energ. 30 (2017) 327–350.
[26] B. Mazhari, An improved solar cell circuit model for organic solar cells, Sol. Energy Mater. Sol. Cells 90 (2006) 1021–1033.
[27] F.A. de Castro, J. Heier, F. Nuesch, R. Hany, Origin of the kink in current-density versus voltage curves and efficiency enhancement of polymer-C_{60} heterojunction solar cells, IEEE J. Sel. Top. Quant. Electron. 16 (2010) 1690–1699.
[28] G. del Pozo, B. Romero, B. Arredondo, Evolution with annealing of solar cell parameters modeling the S-shape of the current–voltage characteristic, Sol. Energy Mater. Sol. Cells 104 (2012) 81–86.
[29] F.J. García-Sánchez, D. Lugo-Muñoz, J. Muci, A. Ortiz-Conde, Lumped parameter modeling of organic solar cells' S-shaped I-V characteristics, IEEE J. Photovolt 3 (2013) 330–335.
[30] F.A. De Castro, A. Laudani, F.R. Fulginei, A. Salvini, An in-depth analysis of the modelling of organic solar cells using multiple-diode circuits, Sol. Energy 135 (2016) 590–597.
[31] E. Sesa, A Novel Electrical Model for Organic Photovoltaic Cells, Ph.D. thesis University of Newcastle, Australia, 2013.
[32] M.M. Furchi, A.A. Zechmeister, F. Hoeller, S. Wachter, A. Pospischil, T. Mueller, Photovoltaics in van der Waals heterostructures, IEEE J. Sel. Top. Quant. Electron. 23 (2017) 106–116.
[33] A. Pozza, G. Bardizza, T. Sample, E. Dunlop, Analysis based on IV curve changes of organic photovoltaic mini-modules subjected to degradation under different temperature and humidity conditions, Proc. 29th Europ. Photovol. Sol. Energy Conf (2014) 1523–1529.
[34] D. White, M. Arai, A. Bittar, K. Yamazawa, A Schottky-diode model of the nonlinear insulation resistance effects in SPRTs—Part 1: Theory, Int. J. Thermophys. 28 (2007) 1843–1854.
[35] K. Yamazawa, M. Arai, D. White, A Schottky-diode model of the nonlinear insulation resistance effects in HRSPRTs—Part 2 Detailed Two-and Three-Wire Measurements, Int. J. Thermophys. 28 (2007) 1855–1867.
[36] A. Gaur, P. Kumar, An improved circuit model for polymer solar cells, Prog. Photovoltaics Res. Appl. 22 (2013) 937–948.
[37] S.K. Rahimian, S. Rayman, R.E. White, Comparison of single particle and equivalent circuit analog models for a lithium-ion cell, J. Power Sources 196 (2011)

8450–8462.
[38] G. Glatting, P. Kletting, S.N. Reske, K. Hohl, C. Ring, Choosing the optimal fit function: comparison of the Akaike information criterion and the F-test, Med. Phys. 34 (2007) 4285–4292.
[39] A. Maurano, R. Hamilton, C.G. Shuttle, A.M. Ballantyne, J. Nelson, B. O'Regan, W.M. Zhang, I. McCulloch, H. Azimi, M. Morana, C.J. Brabec, J.R. Durrant, Recombination dynamics as a key determinant of open circuit voltage in organic bulk heterojunction solar cells: a comparison of four different donor polymers, Adv. Mater. 22 (2010) 4987–4992.
[40] G.A.H. Wetzelaer, M. Kuik, M. Lenes, P.W.M. Blom, Origin of the dark-current ideality factor in polymer:fullerene bulk heterojunction solar cells, Appl. Phys. Lett. 99 (2011) 153506.
[41] K. Tvingstedt, C. Deibel, Temperature dependence of ideality factors in organic solar cells and the relation to radiative efficiency, Adv. Energy Mater 6 (2016) 1502230.
[42] N.C. Giebink, G.P. Wiederrecht, M.R. Wasielewski, S.R. Forrest, Ideal diode equation for organic heterojunctions. I. Derivation and application, Phys. Rev. B 82 (2010) 155305.
[43] U. Würfel, D. Neher, A. Spies, S. Albrecht, Impact of charge transport on current–voltage characteristics and power-conversion efficiency of organic solar cells, Nat. Comms 6 (2015) 6951.
[44] B. Lechene, J. Leroy, O. Tosoni, R. de Bettignies, G. Perrier, Origin of the S-shape upon aging in standard organic solar cells with zinc oxide as transport layer, J. Phys. Chem. C 118 (2014) 20132–20136.
[45] S.R. Cowan, P. Schulz, A.J. Giordano, A. Garcia, B.A. MacLeod, S.R. Marder, A. Kahn, D.S. Ginley, E.L. Ratcliff, D.C. Olson, Chemically controlled reversible and irreversible extraction barriers via stable interface modification of zinc oxide electron collection layer in polycarbazole-based organic solar cells, Adv. Funct. Mater. 24 (2014) 4671–4680.
[46] B. Romero, G. del Pozo, E. Destouesse, S. Chambon, B. Arredondo, Circuital modelling of S-shape removal in the current–voltage characteristic of TiOx inverted organic solar cells through white-light soaking, Org. Electron. 15 (2014) 3546–3551.
[47] A. Gusain, S. Singh, A.K. Chauhan, V. Saxena, P. Jha, P. Veerender, A. Singh, P.V. Vardec, S. Basub, D.K. Aswala, S.K. Gupta, Electron density profile at the interfaces of bulk heterojunction solar cells and its implication on the S-kink characteristics, Chem. Phys. Lett. 646 (2016) 6–11.
[48] K. Tada, Validation of opposed two-diode equivalent-circuit model for S-shaped characteristic in polymer photocell by low-light characterization, Org. Electron. 40 (2017) 8–12.
[49] B. Romero, G. del Pozo, B. Arredondo, D. Martín-Martín, M.P.R. Gordoa, A. Pickering, A. Pérez-Rodríguez, E. Barrena, F.J. García-Sánchez, S-shaped I-V characteristics of organic solar cells: solving Mazhari's lumped-parameter equivalent circuit model, IEEE Trans. Electron. Dev. 64 (2017) 4622–4627.
[50] A. Guerrero, S. Chambon, L. Hirsch, G. Garcia-Belmonte, Light-modulated TiO_x interlayer dipole and contact activation in organic solar cell cathodes, Adv. Funct. Mater. 24 (2014) 6234–6240.
[51] K. Feron, T.J. Nagle, L.J. Rozanski, B.B. Gong, C.J. Fell, Spatially resolved photocurrent measurements of organic solar cells: tracking water ingress at edges and pinholes, Sol. Energy Mater. Sol. Cells 109 (2013) 169–177.